PCCP

# Diffusion in amorphous $LiNbO_3$ studied by $^7Li$ NMR — comparison with the nano- and microcrystalline material†

**Martin Wilkening,[a] Detlef Bork,[b] Sylvio Indris[a] and Paul Heitjans[a]**

[a] *Institut für Physikalische Chemie und Elektrochemie, Universität Hannover, Callinstraße 3-3a, 30167, Hannover, Germany. E-mail: heitjans@mbox.pci.uni-hannover.de*
[b] *Institut für Physikalische Chemie II, Universität Karlsruhe, Kaiserstraße 12, 76128Karlsruhe, Germany*

***Received 1st February 2002, Accepted 28th March 2002***
***First published as an Advance Article on the web 8th May 2002***

Lithium diffusion in amorphous $LiNbO_3$, synthesized by a sol–gel process, was investigated by temperature- and frequency-dependent $^7Li$ NMR experiments. $^7Li$ spin-lattice relaxation rates $T_1^{-1}$ and $^7Li$ nuclear magnetic resonance spectra, in particular line shapes and motional narrowing of the central line, were measured. The results are discussed in comparison with those on nano- and microcrystalline $LiNbO_3$ investigated by us earlier. The Li diffusivity in the amorphous material is much higher than in the microcrystalline one and can be described by practically the same diffusion parameters as in nanocrystalline $LiNbO_3$. This suggests that the diffusion pathways in amorphous $LiNbO_3$ and in the interfacial regions of nanocrystalline $LiNbO_3$ have similar structures.

## 1 Introduction

Lithium niobate, $LiNbO_3$, has attracted substantial scientific and industrial interest in the last decades because of its excellent electro-optical, piezoelectric and acoustic properties.[1,2] The subject of the present work is to study Li dynamics in a homogeneously disordered material, that is amorphous $LiNbO_3$, using nuclear magnetic resonance. The paper is to complement investigations of Li diffusion in nano- and microcrystalline $LiNbO_3$, recently done in our group.‡[3,4] For materials in a homogeneously or heterogeneously disordered state, that is amorphous or, for example, nanocrystalline, often a markedly increased diffusivity as compared to their microcrystalline or single crystalline counterparts is observed. In the three-dimensional ionic conductor $LiNbO_3$ the activation energy for Li diffusion is much lower in the nanocrystalline form than in the microcrystalline material. The Li diffusivity up to 600 K in nanocrystalline $LiNbO_3$ is dominated by the highly mobile ions in the disordered interfacial regions.[3,4]

Nuclear magnetic resonance (NMR) has proven to be a powerful method for the structural elucidation of solids, especially disordered materials.[5] Furthermore NMR is an efficient technique to study diffusion in the solid state and has made significant contributions to the understanding of motions in polymeric and oxide glassy systems, crystalline ceramics and metals. In contrast to other traditional techniques employed for diffusion studies, *e.g.* radioactive tracer or secondary ion mass spectrometry, which are based on the analysis of long-range diffusion, NMR, similar to quasi-elastic neutron scattering, also serves as a probe of local atomic motions.[6]

Spin-lattice relaxation (SLR) measurements as a function of temperature reveal information on short- as well as long-range diffusion. The temperature dependence of the relaxation rate $T_1^{-1}(T)$ for fixed Larmor frequency $\omega_0/2\pi$ is of Arrhenius type here. $T_1$ is related to the mean residence time between successive atomic jumps. The activation energy for short-range diffusion can be determined from the slope of the low-temperature flank of the $T_1^{-1}(T)$ peak.[7] The SLR rates in amorphous $LiNbO_3$ were measured at temperatures from 140 K up to 450 K. For fixed temperature, also frequency dependent SLR measurements were performed between 23 and 78 MHz in order to gain information about the diffusion mechanism prevailing in amorphous $LiNbO_3$. Furthermore, $^7Li$ NMR line shapes and line widths as a function of temperature, *i.e.* motional narrowing (MN), were investigated.

## 2 Experimental

### 2.1 Sample preparation and characterization

**2.1.1 Amorphous sample.** Amorphous lithium niobate was synthesized by a sol–gel process using $LiNb(OEt)_6$ in ethanol as a precursor.[8] A very similar procedure to prepare amorphous $LiNbO_3$ from completely hydrolysed metal alkoxides is described in ref. 9 and 10. To prepare the double alkoxide a solution of $Nb(OEt)_5$ (2M) and LiOEt (2M) in absolute ethanol was refluxed for 1 h in a $N_2$ atmosphere. The $LiNb(OEt)_6$ solution was partially (1/3) hydrolysed with a 2 M water–ethanol solution to a polymer gel and then dried for several hours at 470 K in an oxygen atmosphere. To remove the unhydrolysed alkyls and to prepare amorphous $LiNbO_3$ the dried gel was heat-treated for 5 min at 620 K. The sample obtained by this route still contains organic impurities.

The sample was characterized by time- and temperature-dependent *in situ* X-ray diffraction (XRD) measurements, the morphological structure was observed by scanning electron microscopy (SEM).[8] The amorphous material does not show any diffraction peaks and consists of irregular particles with diameters of 1 to 20 μm. A sample heated at 720 K shows the typical $LiNbO_3$ diffraction pattern.

Furthermore, we investigated the material by differential thermal and thermogravimetric analysis (DTA-TG) and by

† Dedicated to Prof. Dr Hermann Schmalzried on the occasion of his 70th birthday.

‡ In ref. 3 and 4 the microcrystalline form is called polycrystalline $LiNbO_3$.

 DOI: 10.1039/b201193j

differential scanning calorimetry (DSC). The DTA-TG curve of the amorphous sample shows exothermic peaks with weight loss in the temperature range from 680 to 880 K. The peaks are due to the oxidation of organic residuals and crystallization of the material. The DTA-TG curve of a crystalline sample obtained by crystallizing the amorphous material at 720 K, shows no peaks and no weight loss in the temperature range from 300 to 1000 K. The latter result was also found from a DTA analysis of commercially available microcrystalline $LiNbO_3$.

**2.1.2 Micro- and nanocrystalline samples.** The nanocrystalline samples were prepared by high-energy ball milling using a SPEX 8000 ball mill with an alumina vial set.[3,4,11,12] The source material was microcrystalline lithium niobate (Aldrich) consisting of irregularly shaped crystallites with grain size in the range from 0.6 to 6 μm. By varying the milling time from 0.5 to 128 h samples with average grain sizes of 100 to 20 nm were obtained. Grain sizes were determined from the broadening of the XRD lines. In addition to XRD the samples were characterized by DSC and transmission electron microscopy (TEM) measurements. A 16 h ball milled sample with an average particle size of 23 nm was chosen for detailed NMR investigations. It shows more regularly shaped grains compared to the microcrystalline material. The nanometer sized grains are separated by large-angle grain boundaries. Consequently there is no correlation between the crystallographic orientations of neighbouring grains.

### 2.2 NMR measurements—technique and setup

All NMR measurements (SLR rates and $^7$Li spectra) on amorphous $LiNbO_3$ were carried out with a Bruker MSL 100 console with a Kalmus LP 400 high-frequency amplifier in connection with a tunable (0–8 T) Oxford cryomagnet (89 mm wide bore). In the temperature range from 140 K to 450 K a commercial Bruker probe head was employed. The temperature was stabilized within 0.5 K using a gas flow of freshly evaporated nitrogen or a stream of heated air. The NMR experiments had to be restricted to temperatures below 450 K in order to avoid crystallization of the amorphous sample (*cf.* section 2.1).

The $^7$Li SLR rates were determined using the saturation recovery pulse sequence.[13] The 90° pulse lengths were 2.7 μs, 3.5 μs and 5.0 μs at NMR frequencies $\nu = \omega_0/2\pi$ of 23 MHz, 39 MHz and 78 MHz. The magnetization

$$M(\tau) = M_0\left\{1 - \exp\left(-\frac{\tau}{T_1}\right)\right\} \qquad (1)$$

was recorded for 30 different $\tau$ values. The variable waiting time $\tau$ ranged from 0.5 s to 80 s. Each data point of the magnetization curve $M(\tau)$ was obtained by the integral over the free induction decay (FID). 16 to 32 transients were accumulated for each FID.

The $^7$Li NMR spectra of amorphous $LiNbO_3$ were recorded at 78 MHz. They were acquired with a single $\pi/2$ pulse. Typically 16 scans were added up and then Fourier transformed.

SLR rates of nano- and microcrystalline $LiNbO_3$, investigated by our group,[3,4] were recorded also using a Bruker MSL 100 spectrometer. $T_1$ experiments at 78 MHz, the acquisition of the $^7$Li spectra and investigation of MN of the nano- and microcrystalline material were performed using a Bruker MSL 200 console with an internal 200 W amplifier and an Oxford cryomagnet at fixed field. For measurements above 500 K in the case of microcrystalline $LiNbO_3$, a special home-built high-temperature probe head was used.

## 3 Results

### 3.1 Spin-lattice relaxation

The evolution of the magnetization $M(\tau)$ in amorphous $LiNbO_3$ can be fitted by a single exponential. In Fig. 1 the spin-lattice relaxation rate of amorphous $LiNbO_3$ at three Larmor frequencies (23, 39 and 78 MHz) is shown as a function of inverse temperature. While the pronounced low-temperature (lT) side of the diffusion-induced peak is clearly detected, the SLR rate maximum and the high-temperature side cannot be reached in the experimentally accessible temperature range up to 450 K. $T_1^{-1}(T^{-1})$ consists of a superposition of a diffusion-induced contribution and a nondiffusional background which shows up at temperatures below 250 K. To obtain the purely diffusion-induced data $T_{1\,\mathrm{diff}}^{-1}$, the background (bgr) rate, which can be described by an empirical power law $T_{1\,\mathrm{bgr}}^{-1} \propto T^{\gamma}$, is extrapolated to higher temperatures (*cf.* Fig. 1) and subtracted from the measured data

$$T_{1\,\mathrm{diff}}^{-1} = T_1^{-1} - T_{1\,\mathrm{bgr}}^{-1}. \qquad (2)$$

The exponent $\gamma$ describes the temperature dependence of the background rate and ranges from 1.6 to 2.0 in amorphous $LiNbO_3$ in the observed frequency range (23, 39, 78 MHz). At a given temperature in the range from 140 K to 230 K the frequency dependence of the background rate can be described by $T_{1\,\mathrm{bgr}}^{-1} \propto \nu^{-\beta}$ with $\beta = 1.4 \pm 0.1$. This behavior of $T_{1\,\mathrm{bgr}}^{-1}$ may be ascribed to the presence of paramagnetic impurities.[14] The slope of the diffusion induced peak yields the low-temperature activation energy $E^{\mathrm{lT}}$.[7] The flank may be described by an Arrhenius law

$$T_{1\,\mathrm{diff}}^{-1} \propto \exp\left(-\frac{E^{\mathrm{lT}}}{k_{\mathrm{B}}T}\right). \qquad (2)$$

$k_{\mathrm{B}}$ is the Boltzmann constant. The activation energy $E^{\mathrm{lT}}$ determined from the SLR data is nearly independent of the frequency (*cf.* Fig. 1) and amounts to about 0.27 eV.

Fig. 2 displays the SLR rates of the amorphous material at 23 MHz in comparison with the results of micro- and nanocrystalline $LiNbO_3$ measured at 24 MHz. Analogous results

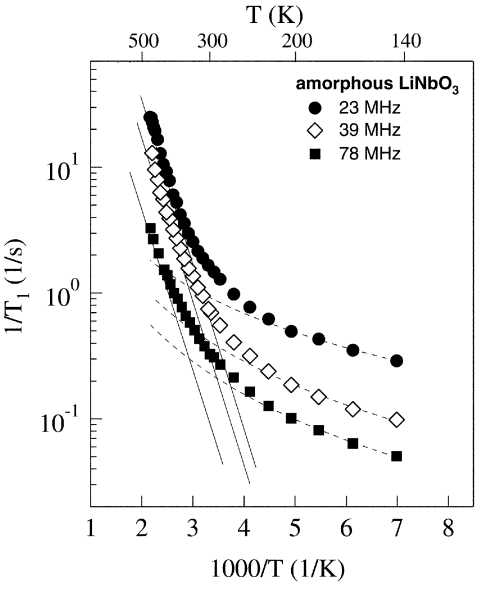


**Fig. 1** Arrhenius diagram representing the temperature dependence of the $^7$Li SLR $T_1^{-1}$ rate in amorphous $LiNbO_3$ at three different Larmor frequencies. The dashed lines show fits to the background SLR rates using a power law. The background rate is extrapolated to higher temperatures and subtracted from the measured data $T_1^{-1}$ to obtain $T_{1\,\mathrm{diff}}^{-1}$. The solid lines represent fits to $T_{1\,\mathrm{diff}}^{-1}$. The data points $T_{1\,\mathrm{diff}}^{-1}(1/T)$ calculated from eqn. (2) are not shown.

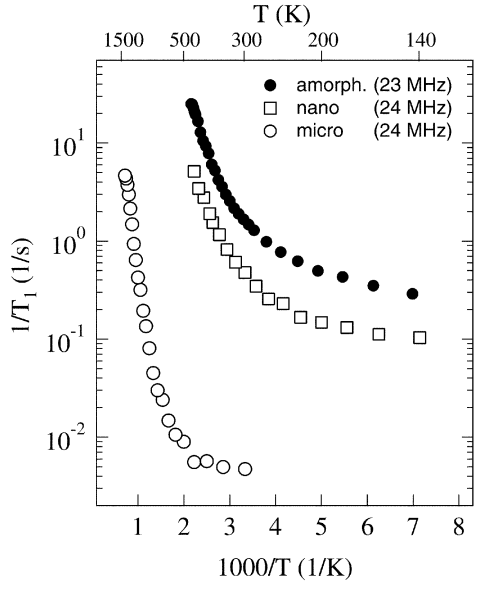


**Fig. 2** Temperature dependence of the $^7$Li SLR rate $T_1^{-1}$ in amorphous $LiNbO_3$ compared with nano- and microcrystalline $LiNbO_3$. The data for nano- and microcrystalline $LiNbO_3$ were taken from ref. 3.

were obtained at 39 and 78 MHz. The diffusion induced peak for microcrystalline $LiNbO_3$ is shifted to higher temperatures. $T_{1\,\mathrm{diff}}^{-1}$ is proportional to $\tau_c^{-1}$ characterizing the motional correlation rate which is directly related to the mean jump rate. At a fixed temperature $T$ the SLR rate $T_1^{-1}(T)$, *i.e.* also $\tau_c^{-1}$, rises and the Li ions increasingly become more mobile in the material order: microcrystalline, nanocrystalline, amorphous, where the mobility appears to be similar in the latter two cases. For example, in the nanocrystalline and the amorphous material the steep increase of $T_1^{-1}(T)$ starts at about 300 K whereas in the microcrystalline material no more than the background rate is detected at this temperature. In the case of microcrystalline $LiNbO_3$ the background rate is nearly temperature independent. The background rate in the nanocrystalline material can be fitted by a power law $T_{1\,\mathrm{bgr}}^{-1} \propto T^{\gamma}$ with $\gamma = 1.1$ for 23 MHz. At 39 MHz and 78 MHz $\gamma$ is 1.5 and 1.3, respectively. The activation energies determined from the $T_{1\,\mathrm{diff}}^{-1}$ data, obtained by the correction procedure mentioned above, are summarized in Table 2. The activation energy characterizing the short-range Li diffusion in amorphous $LiNbO_3$ (0.27 eV) is practically the same as the activation energy in nanocrystalline $LiNbO_3$ (0.28 eV, 16 h ball milled sample).[3,4]

It is worth noting that, in general, small deviations from ideal stoichiometry in certain oxides can have an appreciable effect on the ionic diffusivity.[15] However, in the case of $LiNbO_3$ single crystals it is reported that the conductivity near 1 atm $O_2$ pressure does not depend on oxygen concentration at temperatures lower than 1200 K.[16] Therefore deviation from stoichiometry does not dominate conduction in this range of temperature and pressure. In our work, the nanocrystalline samples were prepared from the microcrystalline material (*cf.* section 2.1) and the microcrystalline sample is used as a reference system. In this context we also have investigated microcrystalline $LiNbO_3$, which was obtained by crystallizing the amorphous material for several hours at about 750 K. The $T_1^{-1}(T)$ behavior and the MN of the $^7$Li NMR line with increasing temperature are in fair agreement with the NMR results from commercially available microcrystalline $LiNbO_3$ ($E^{\mathrm{lT}} = 0.77$ eV) investigated in ref. 3 and 4 and shown here.

The frequency dependence of the $^7$Li SLR rates in the temperature regime of the diffusion-induced low-temperature flank in Fig. 1 can be described by a power law

$$T_{1\,\mathrm{diff}}^{-1} \propto \nu^{-\alpha}. \quad (4)$$

For amorphous $LiNbO_3$ $\alpha$ is $1.7 \pm 0.2$. The exponent $\alpha$ is 1.1 and 1.2 for the nano- and microcrystalline material, respectively. Ideal Bloembergen–Purcell–Pound (BPP)[17] behavior, incorporating random isotropic diffusion, would imply $\alpha = 2$. $\alpha \approx 1.7$ indicates the influence of structural disorder and/or coulomb interactions between the hopping ions assumed by various models.[18–20]

In glassy $LiNbO_3$, prepared by rapid twin-roller quenching, the Li conductivity $\sigma_{\mathrm{DC}}$ was found to be about $10^{20}$ times greater than in the single crystal at room temperture.[21] The activation energy $E^{\sigma_{\mathrm{DC}}}$ turned out to be about 0.4 eV. $E^{\sigma_{\mathrm{DC}}}$ can be identified with $E^{\mathrm{hT}}$ of the high-temperature side of $T_{1\,\mathrm{diff}}^{-1}(T)$. The ratio $E^{\mathrm{lT}}/E^{\mathrm{hT}}$ should be related to the exponent $\alpha$ by[7]

$$E^{\mathrm{lT}}/E^{\mathrm{hT}} = \alpha - 1. \quad (5)$$

Inserting $E^{\mathrm{lT}} = 0.27$ eV and $E^{\mathrm{hT}} = 0.4$ eV yields $\alpha = 1.7$. This value agrees with the result directly obtained from the frequency dependence of the SLR rate data fitted by eqn. (4). Amorphous $LiNbO_3$, prepared from completely hydrolysed $LiNb(OEt)_6$, indicates a similar activation energy $E^{\sigma_{\mathrm{DC}}}$ of 0.47 eV.[9] This leads to a frequency dependence $\alpha = 1.6$. Though results for amorphous materials prepared by diverse methods are expected to differ, the interpretation of these small differences in $\alpha$ is expected to be beyond the scope of the underlying models.

### 3.2 NMR spectra and motional narrowing

**3.2.1 NMR spectra—line shapes.** As reported and discussed in ref. 4, the central line of the $^7$Li ($I = 3/2$) NMR spectra in nanocrystalline $LiNbO_3$ reveals a superposition of two contributions: a narrow component which is caused by the ions in the disordered interfacial regions and a broad contribution which can be allocated to the Li ions in the grains. The ratio of the area under the narrow line to that under the total area, which is about 23%, corresponds to the fraction of atoms that can be ascribed to the interfacial regions.[4] Due to the static electric field gradient at a Li site in $LiNbO_3$ resulting from the non-cubic crystal symmetry, the quadrupolar splitting of $^7$Li is not averaged out with increasing temperature. Provided the respective Li sites are equivalent, for both the static and mobile Li components of the NMR line, the central transition alone is observed. The central transition in the NMR spectra of the amorphous and the microcrystalline material can be described with a homogeneous line, which can be represented by a single gaussian at low temperatures and by a single lorentzian at high temperatures. In Fig. 3 the $^7$Li spectra of amorphous $LiNbO_3$ and, for comparison, the spectra of nano- and microcrystalline $LiNbO_3$ are shown for various temperatures.

At higher temperatures, *viz.* $T > 400$ K, also the $^7$Li NMR central transition line of microcrystalline $LiNbO_3$ seems to decompose into a broad gaussian and a narrow lorentzian contribution. However, the area fraction of the narrow contribution is only 1–2%. It has negligible influence on our results and will not further be discussed here. Xia *et al.*[22] have studied structure and dynamics in crystalline $(LiNbO_3)_{1-x} - (WO_3)_x$ solid solutions using $^7$Li and $^6$Li NMR. The $^7$Li spectra for $x = 0$ reveal two distinct contributions to the NMR line, too. The area fraction of the narrow contribution was found to be 0.6% at 470 K in agreement with our result.

**3.2.2 Motional narrowing.** Fig. 4 displays the motional narrowing of the line width (fwhm) of the central transition in the $^7$Li NMR spectra of the amorphous, nano- and microcrystalline materials at a resonance frequency of 78 MHz. To deter-

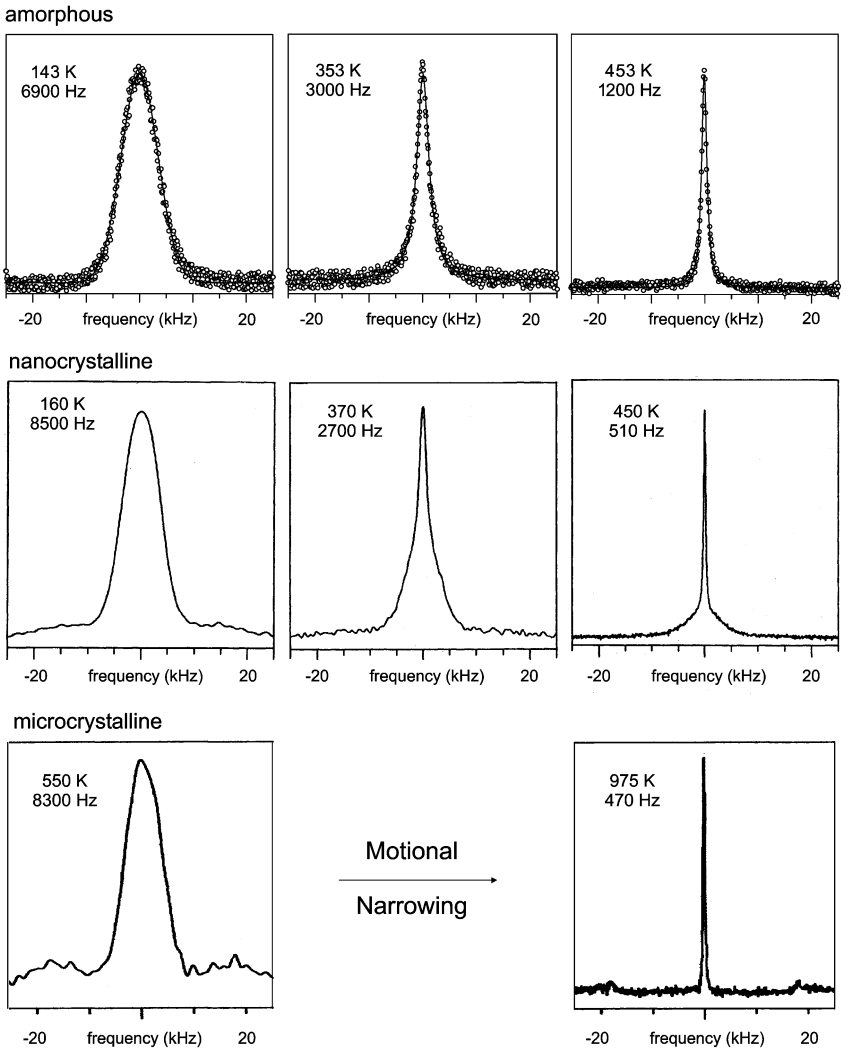


**Fig. 3** $^{7}$Li NMR spectra of amorphous, nano- and microcrystalline $LiNbO_3$ at various temperatures. The data for nano- and microcrystalline $LiNbO_3$ were taken from ref. 4.

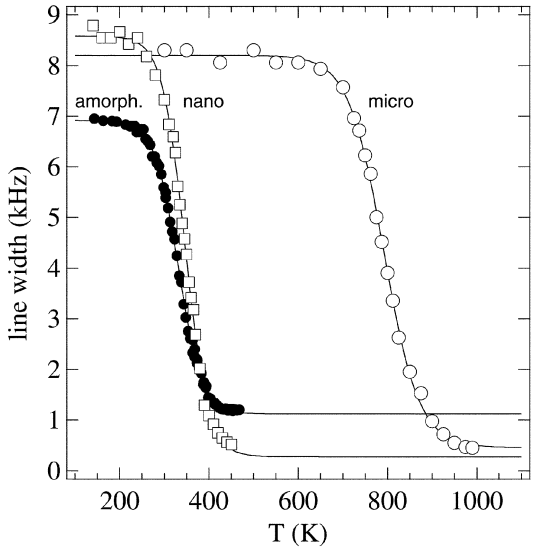


**Fig. 4** Full width at half-maximum of the central transition line in the $^{7}$Li-NMR spectra of amorphous, nano- and microcrystalline $LiNbO_3$ obtained at 78 MHz as a function of temperature. The data for nano- and microcrystalline $LiNbO_3$ were taken from ref. 4. The lines represent fits by eqn. (6).

mine the effective line widths of nanocrystalline $LiNbO_3$ the $^{7}$Li NMR line is fitted with a single gaussian or lorentzian; the two contributions of the NMR line have not been separated. The temperature-dependent narrowing of the line width in amorphous lithium niobate is similar to the MN in the nanocrystalline material. In both cases MN starts at about 300 K, that is 400 K below the onset temperature in the microcrystalline sample. Thus the Li ions in the disordered interfacial regions become mobile at the same temperature as the Li ions in the amorphous material. At 480 K MN of amorphous and nanocrystalline $LiNbO_3$ is completed, whereas the Li ions in the microcrystalline material, and hence also in the grains of the nanocrystalline material, are still immobile. The onset of MN in microcrystalline $LiNbO_3$ occurs at about 650 K.

The larger residual line width at high temperatures in the case of the amorphous sample is due to the fact that the field inhomogeneity of the magnet was higher than that used to determine the MN of nano- and microcrystalline $LiNbO_3$. The low-temperature value of the $^{7}$Li linewidth in the static limit is smaller for the amorphous sample than for the micro- or the nanocrystalline sample. Regarding the Van Vleck formula[14] this may be attributed to a larger mean value of atomic distances in an amorphous material compared to a microcrystalline sample.

In addition to the SLR measurements, examination of MN represents another method, sometimes considered to be less

reliable, to determine the activation energy for the Li diffusion. The fits in Fig. 4 refer to the following function given in ref. 23.

$$\Delta\nu(T) = \Delta\nu_R\left[1 + \left(\frac{\Delta\nu_R}{B} - 1\right)\exp\left(-\frac{E^{\mathrm{MN}}}{k_{\mathrm{B}}T}\right)\right]^{-1} + D \quad (6)$$

$\Delta\nu(T)$ is the line width of the central transition at temperature $T$, $\Delta\nu_R$ and $B$ are parameters, attributed to the line widths of the rigid lattice and the thermally activated ions,[23] respectively. $D$ is a temperature-independent line width caused, *e.g.*, by the inhomogeneity of the external static magnetic field. The parameters used for fitting eqn. (6) to the data of Fig. 4 are listed in Table 1.

In ref. 4 the apparent activation energies for nano- and microcrystalline $LiNbO_3$ were calculated *via* the *ad hoc* formula:[14]

$$\Delta\nu(T) = \sqrt{\Delta\nu_R^2\frac{2}{\pi}\arctan\left[\sigma\Delta\nu(T)\tau_\infty\exp\left(\frac{E^{\mathrm{MN}}}{k_{\mathrm{B}}T}\right)\right] + \Delta\nu_\infty^2} \quad (7)$$

$\sigma$ is a fit parameter here chosen to be one. $\tau_\infty$ is the pre-exponential factor in the Arrhenius relation assumed for the temperature dependence of the correlation time $\tau_c$, and $\Delta\nu_\infty$ is the residual line width caused by nondipolar interactions when MN is completed.

A third way to estimate the activation energy from MN data is provided by the empirical Waugh–Fedin[24] expression:

$$E^{\mathrm{MN}}/\mathrm{eV} = 1.617\times10^{-3}\cdot T_c/\mathrm{K} \quad (8)$$

$T_c$ is the onset temperature of MN. The Waugh–Fedin method is useful if only the onset of MN can be located and the full range of MN cannot be determined. The activation energies obtained from MN data are listed in Table 2. Being consistent with the results from SLR measurements, $E^{\mathrm{MN}}$ of amorphous $LiNbO_3$ is similar to the activation energy of nanocrystalline $LiNbO_3$, whereas the microcrystalline form shows a higher activation energy $E^{\mathrm{MN}}$. Xia *et al.*[22] derived from MN data *via* eqn. (8) an activation energy of about 1 eV for the Li diffusivity in $(LiNbO_3)_{1-x}-(WO_3)_x$ crystals for $x = 0$. This is in agreement with our result.

## 4 Discussion

Nanocrystalline materials are mostly regarded as heterogeneously structured systems consisting of randomly orientated crystallites with ideal crystal structure and heavily disordered, maybe amorphous, interfacial regions of about 0.5 to 1 nm thickness with reduced density and coordination number.

**Table 1** Parameters used for fitting eqn. (6) to the data of Fig. 4

| | $\Delta\nu_R$/kHz | $B$/kHz | $D$/kHz | $E^{\mathrm{MN}}$/eV |
|---|---|---|---|---|
| Amorphous | 5.97 | $2.22\cdot10^{-5}$ | 0.95 | 0.35 |
| Nano | 8.35 | $1.76\cdot10^{-5}$ | 0.26 | 0.39 |
| Micro | 7.64 | $1.31\cdot10^{-7}$ | 0.50 | 1.25 |

**Table 2** Activation energies of short-range Li diffusion in amorphous, nano- and microcrystalline $LiNbO_3$ obtained from SLR and MN data. The activation energies calculated *via* eqn. (7) are taken from ref. 4. The error is typically 2 in the last digit

| | | MN: $E^{\mathrm{MN}}$/eV | | |
|---|---|---|---|---|
| | SLR: $E^{\mathrm{IT}}$/eV | Eqn. (6) | Eqn. (7) | Eqn. (8) |
| Amorphous | 0.27 | 0.35 | — | 0.36 |
| Nano | 0.28 | 0.39 | 0.26 | 0.40 |
| Micro | 0.77 | 1.25 | 0.83 | 1.07 |

In an amorphous material there is a broad distribution of the heights of potential energy barriers contrary to that in the corresponding crystalline structure with equal potential energy barriers. The ions in an amorphous phase tend to preferentially follow diffusion pathways with lower energy barriers. Consequently, the self-diffusion of, *e.g.*, small Li ions should be enhanced compared to a coarse grained crystalline material as a reference system. In fact, SLR measurements and MN data show that the Li ions in the amorphous phase are highly mobile at low temperatures compared to the ions in microcrystalline $LiNbO_3$. The activation energy in amorphous $LiNbO_3$ is about 1/3 of the value obtained for the microcrystalline material.

When describing a nanocrystalline system as a heterogeneous mixture of a crystalline and an amorphous phase and following the mentioned reasoning, one may suppose that in a three-dimensional nanocrystalline ionic conductor: (i) the Li diffusivity should be dominated by the ions in the disordered interfacial regions[3,4]; and (ii) be comparable to the diffusivity in the purely amorphous material. In the case of lithium niobate the present NMR measurements confirm these expectations. The activation energies of amorphous (0.27 eV) and nanocrystalline $LiNbO_3$ (0.28 eV) are nearly the same, whereas for microcrystalline $LiNbO_3$ a much higher activation energy (0.77 eV) is obtained from SLR measurements. Clearly, the Li jump rates in the amorphous material are much higher than in the microcrystalline one.

In contrast to the results for $LiNbO_3$, the activation energies for nano- and microcrystalline $Li_xTiS_2$ obtained recently also by our group from $T_1$ measurements[25] are very similar (0.16 eV and 0.19 eV) and much higher than in the amorphous sample (0.07 eV). To explain this deviating behavior, the layered structure of hexagonal $Li_xTiS_2$ which is a two-dimensional fast ionic conductor has to be taken into account. The results can be ascribed to pathway formation on the surface of the nano-grains. These surface pathways are the dominant track for mobile ions.[25] The nano-grains appear to be disk-like shaped and not spherical-like as in $LiNbO_3$.[26]

The decomposition of the central line of nanocrystalline $LiNbO_3$ into a broad and a narrow component is due to two different Li species in the sample and shows the heterogeneous structure of the material. The two different Li reservoirs may be ascribed to the Li ions in the grains and the highly mobile ions in the interfacial regions. In the whole experimentally accessible temperature range the amorphous material shows only a single-structured central $^7$Li NMR line, which can be fitted by a single lorentzian or gaussian function and which agrees with the narrow component of nanocrystalline $LiNbO_3$ comparing line shapes as a function of temperature and MN of both samples. MN in the amorphous and nanocrystalline material is completed 200 K below the temperature where it starts in the microcrystalline form. At even higher temperature, that is about 600 K, also the broad component of the nanocrystalline material should start to narrow.

In view of all these results we may conclude that there are similar diffusion pathways in the purely amorphous material and in the disordered interfaces in nanocrystalline $LiNbO_3$. Thus interfacial regions in nanocrystalline $LiNbO_3$ seem to have amorphous-like structure.

## 5 Conclusion

Li diffusion in amorphous $LiNbO_3$ was studied by temperature and frequency-dependent spin-lattice relaxation measurements and investigation of motional narrowing of the central $^7$Li NMR line in the temperature range from 140 K to 450 K. The results were compared to those obtained from NMR experiments on nano- and microcrystalline $LiNbO_3$. In amorphous $LiNbO_3$ the activation energy for short-range Li motion

obtained from the low-temperature flank of the peak of the spin-lattice relaxation rate is about 0.27 eV. It is practically the same as the activation energy of nanocrystalline $LiNbO_3$ which is about 1/3 of the value obtained for microcrystalline $LiNbO_3$. The frequency dependence of the spin-lattice relaxation rate shows non-BPP behavior for all samples. The $^7Li$ NMR line of the amorphous sample consists of a homogeneous line which can be described by a single gaussian (low temperatures) or lorentzian (high temperatures). The $^7Li$ NMR line of nanocrystalline $LiNbO_3$ is composed of a broad component (Li ions in the grains) and a narrow component (Li ions in the interfacial regions). MN of the $^7Li$ NMR line in the amorphous material is very similar to that in the nanocrystalline form, whereas the onset of MN in microcrystalline $LiNbO_3$ is shifted by 400 K to higher temperatures.

In summary, the Li diffusivity in amorphous $LiNbO_3$ is much higher than that in the microcrystalline form. Our results show similar diffusion pathways in amorphous and nanocrystalline $LiNbO_3$. Consequently, we found indications of an amorphous structure of the interfacial regions in nanocrystalline $LiNbO_3$.

## Acknowledgement

We are grateful to Dr M. Dinges and Prof. H. Fueß (Technische Universität Darmstadt) for supplying amorphous $LiNbO_3$ samples and the Deutsche Forschungsgemeinschaft for financial support. P. H. would also like to acknowledge financial help by the Fonds der Chemischen Industrie.

## References

1 R. S. Weis and K. Gaylord, *Appl. Phys.*, 1985, **A37**, 191.
2 A. Räuber, in *Current Topics in Materials Science*, ed. E. Kaldis, Publishing Company, vol. 1, 1978.
3 D. Bork and P. Heitjans, *J. Phys. Chem. B*, 1998, **102**, 7303.
4 D. Bork and P. Heitjans, *J. Phys. Chem. B*, 2001, **105**, 9162.
5 H. Eckert, in *Insulating and Semiconducting Glasses*, ed. P. Boolchand, World Scientific Press, Singapore, 2000.
6 *Diffusion in Condensed Matter*, ed. J. Kärger, P. Heitjans and R. Haberlandt, Springer, Berlin, 1998.
7 P. Heitjans and A. Schirmer, in *Diffusion in Condensed Matter*, ed. J. Kärger, P. Heitjans and R. Haberlandt, Springer, Berlin, 1998.
8 M. Dinges, PhD Thesis, Technische Hochschule Darmstadt, 1997, and private communication.
9 S. Ono, H. Mochizuki and S. Hirano, *J. Ceram. Soc. Jpn.*, 1996, **104**, 574.
10 S. Hirano and K. Kato, *Adv. Ceram. Mater.*, 1987, **2**, 142.
11 S. Indris, D. Bork and P. Heitjans, *J. Mat. Synthesis and Processing*, 2000, **8**, 245.
12 D. Bork, PhD Thesis, Universität Hannover, 1997.
13 E. Fukushima, S. B. W. Roeder, *Experimental Pulse NMR*, Addison-Wesley, Reading, 1981.
14 A. Abragam, *The Principles of Nuclear Magnetism*, Oxford University Press, Oxford, 1999.
15 H. Schmalzried, *Chemical Kinetics of Solids*, VCH, Weinheim, 1995.
16 G. Bergmann, *Solid State Commun.*, 1968, **6**, 77.
17 N. Bloembergen, E. M. Purcell and R. V. Pound, *Phys. Rev.*, 1948, **73**, 679.
18 K. L. Ngai and O. Kanert, *Solid State Ionics*, 1992, **53**, 963.
19 K. Funke, *Prog. Solid State Chem.*, 1993, **22**, 11.
20 A. Bunde, P. Maass and M. Meyer, in *Diffusion in Condensed Matter*, ed. J. Kärger, P. Heitjans and R. Haberlandt, Springer, Berlin, 1998.
21 A. M. Glass, K. Nassau and T. J. Negran, *J. Appl. Phys.*, 1978, **49**, 4808.
22 Y. Xia, N. Machida, X. Wu, Ch. Lakeman, L. van Wüllen, F. Lange, C. Levi and H. Eckert, *J. Phys. Chem. B*, 1997, **101**, 9180.
23 J. R. Hendrickson and P. J. Bray, *J. Magn. Res.*, 1973, **9**, 341.
24 J. S. Waugh and E. I. Fedin, *Sov. Phys. Solid State*, 1963, **4**, 1633.
25 R. Winter and P. Heitjans, *J. Phys. Chem. B*, 2001, **105**, 6108.
26 R. Winter and P. Heitjans, *J. Non-Cryst. Solids*, 2001, **293–295**, 19.